Magnetic phases in Ge–Fe thin films containing high Fe content

2006 J. Phys.: Condens. Matter 18 11263

(http://iopscience.iop.org/0953-8984/18/49/018)

INSTITUTE OF PHYSICS PUBLISHING JOURNAL OF PHYSICS: CONDENSED MATTER

J. Phys.: Condens. Matter **18** (2006) 11263–11274 doi:10.1088/0953-8984/18/49/018

Magnetic phases in Ge–Fe thin films containing high Fe content

S H Song[1], **M H Jung**[2] **and S H Lim**[3,4]

[1] Materials Science and Engineering, Iowa State University, Ames, IA 50011-3020, USA
[2] Quantum Material Research Team, Korea Basic Science Institute, 52 Yeoeun-dong, Yusung-gu, Daejeon 305-333, Korea
[3] Department of Materials Science and Engineering, Korea University, Anam-dong, Seongbuk-gu, Seoul 136-713, Korea

E-mail: sangholim@korea.ac.kr

Received 18 August 2006, in final form 25 October 2006
Published 22 November 2006
Online at stacks.iop.org/JPhysCM/18/11263

Abstract

Magnetic phases in evaporated thin films of $Ge_{100-x}Fe_x$ (x in at.%) alloys with $x = 36.6$ and 51.8 are examined. At $x = 36.6$, a single amorphous phase is formed. The magnetic phase at room temperature appears to be ferromagnetic, and it transforms into a spin-glass phase at 20 K. The magnetic phases are more complicated at the higher Fe composition of $x = 51.8$, which is mainly due to the presence of Fe precipitates in the amorphous matrix. An analysis based on the superparamagnetism indicates that the effective composition of the amorphous phase is estimated to be $x = 39.4$, and this amorphous phase shows a similar magnetic behaviour to that observed in the $x = 36.6$ sample with the exception of a slightly higher spin freezing temperature of 30 K. Due to the Fe precipitates, an additional superparamagnetic behaviour is observed with a blocking temperature of 160 K. Magnetization saturation in the spin-glass state occurs at a relatively small applied field, which indicates that the direct antiferromagnetic exchange coupling between Fe ions is weak.

(Some figures in this article are in colour only in the electronic version)

1. Introduction

Group IV based diluted magnetic semiconductors (DMSs) have been predicted to have high Curie temperatures from theory based on the Zener model [1]. Among the group IV semiconductors, Ge has been most intensively studied. Park *et al* reported encouraging results from epitaxial Ge–Mn thin films deposited by molecular beam epitaxy (MBE) [2]. Ferromagnetic ordering at reasonably high Curie temperatures has been reported. Choi *et al* also reported ferromagnetic order in bulk Ge–Cr crystals [3], but this was not confirmed in a

[4] Author to whom any correspondence should be addressed.

Table 1. The thickness of the thin films investigated in this work.

x (at.%)	Film thickness (nm)
0	145
5.1	190
11.0	77
12.5	80
14.5	96
16.0	130
36.6	75
51.8	150

later work by Kioseoglou *et al* in thin films deposited by MBE [4]. Despite these successes, ferromagnetic ordering at room temperature has not been realized. In the case of Ge–Mn thin films made by MBE, the highest Curie temperature reported was 116 K [2]. The main reason for the low Curie temperature might be the limited solubility of 'magnetic' transition metals (TMs) incorporated into Ge. One effort to extend the solubility limit was to use a low-temperature MBE. Even with this process, the solubility of magnetic elements was typically less than 4 at.% [2, 4]. It is believed that this problem can be solved in a more fundamental way by forming an amorphous phase.

In a series of experiments, the magnetic and transport properties of evaporated thin films of Ge–Cr [5], Ge–Mn [6], and Ge–Fe [7] were investigated. In all cases, it was possible to incorporate a large amount of the transition metals without forming second phases. Consequently, ferromagnetic ordering appeared to occur at room temperature in well-characterized samples over a wide composition range. Potentially, this has significant practical importance in spintronics, although some more work on spin polarization, for example, needs to be carried out in the future. In addition to the practical importance of these new materials, interesting magnetic properties were also observed. One example is the observation of a spin-glass behaviour in amorphous Ge–Mn thin films at low temperatures [8]. This study examined the magnetic properties of amorphous Ge–Fe thin films with particular emphasis being placed on identifying the different magnetic phases in the alloys with a high Fe content.

2. Experimental method

$Ge_{100-x}Fe_x$ (x in at.%) thin films with a thickness of approximately 100 nm were prepared by thermal co-evaporation onto oxidized Si at room temperature. The thickness of the SiO_2 layer was 100 nm (0.1 μm) and that of Si was 200 μm. The base pressure was $<2 \times 10^{-6}$ Torr. The film thickness was measured using a profilometer. The microstructure was examined by x-ray diffraction (XRD) using Cu Kα radiation and high-resolution transmission electron microscopy (HRTEM). The composition was determined by Rutherford backscattering. A superconducting quantum interference device (SQUID) and an alternating gradient magnetometer (AGM) were used for magnetic characterization under static conditions. The magnetic susceptibility under ac conditions was measured using a physical properties measurement system (PPMS) over a wide frequency range of 0.5–10 kHz. The magnetic measurements were carried out down to liquid helium temperature.

3. Results and discussion

The thickness of the thin films investigated in this work, which is summarized in table 1, is in the range 75–190 nm. XRD and HRTEM were used to characterize the microstructure of

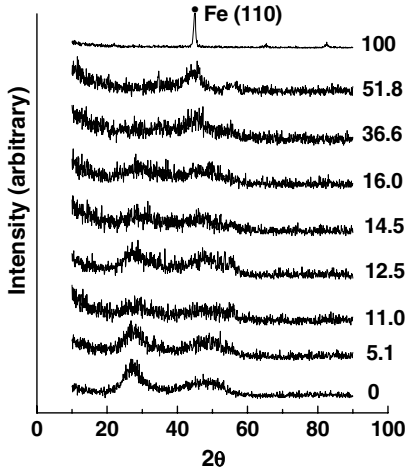

Figure 1. X-ray diffraction patterns of $Ge_{100-x}Fe_x$ thin films over a wide composition range from pure Ge ($x = 0$) to pure Fe ($x = 100$). The number at each diffraction pattern denotes x, the Fe content in at.%.

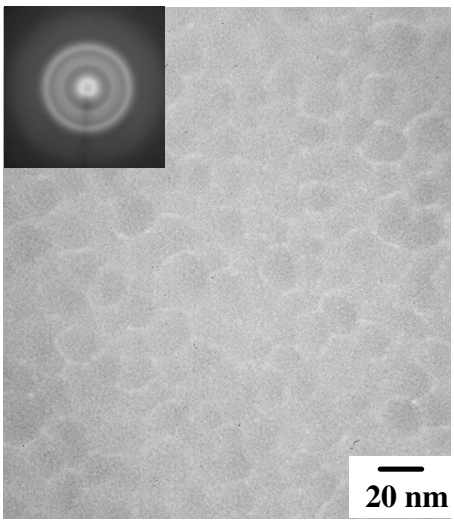

Figure 2. An HRTEM image and an SAD pattern (inset) for the sample with $x = 36.6$.

the fabricated thin films. Figure 1 shows the XRD patterns over a wide composition range from $x = 0$ to 100. The possible compounds in the binary Ge–Fe system were reported to be $FeGe_2$, FeGe, Fe_6Ge_5, and Fe_3Ge [9], of which none are magnetic [9]. No obvious crystalline peaks were observed from the x-ray diffraction results with the exception of the pure Fe sample ($x = 100$), where a sharp diffraction peak was observed at $2\theta = 45°$, corresponding to the Fe{110} planes. In pure Fe, there are two much weaker peaks at $2\theta = 64°$ and 83°, which correspond to Fe{200} and Fe{211}, respectively. It is noted that the main focus of this study was on the two samples containing a high Fe concentration, $x = 36.6$ and 51.8.

HRTEM was used to further examine the microstructure of these two samples. Figure 2 shows the HRTEM image for the sample with $x = 36.6$. The selected area diffraction (SAD)

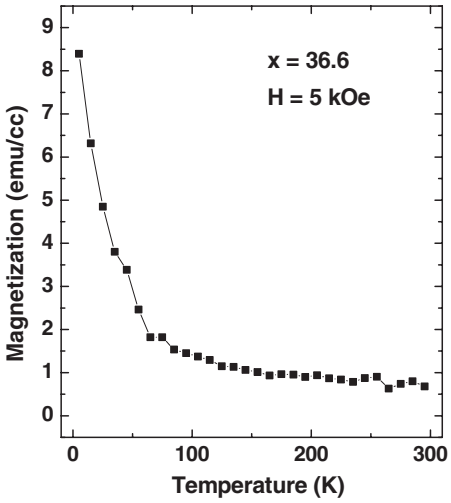

Figure 3. An M–T curve measured with a SQUID at temperatures ranging from 4 to 300 K for the sample with $x = 36.6$. The result was obtained at the zero-field-cooled condition and at an applied field of 5 kOe.

pattern is also shown in the inset of the figure. An analysis of the results shows that the microstructure consists of a single amorphous phase. Significant effort was made to examine the microstructure of the sample with the highest Fe content ($x = 51.8$) by HRTEM, but no satisfactory results were obtained. The sample was too brittle to do sample preparation for HRTEM possibly due to the formation of Fe precipitates, which was confirmed later by magnetic characterization.

Figure 3 shows the magnetization versus temperature (M–T) curve for the sample with $x = 36.6$ measured with a SQUID at temperatures ranging from 4 to 300 K. The sample was first cooled without applying a magnetic field (the zero-field-cooled condition) and magnetization was measured at an applied magnetic field of 5 kOe as a function of the sample temperature. The M–T curve shown in figure 3 does not show the usual Brillouin behaviour. As the temperature increases from 4 K, there is a significant decrease in magnetization in the low-temperature range, which is followed by a slow decrease in magnetization at higher temperatures. This temperature dependence results in a concave shape of the M–T curve. Indeed, a similar behaviour was previously reported [2] and predicted theoretically [10]. For the same sample, the magnetization versus applied magnetic field (M–H) curves were measured at two different temperatures of 5 K and room temperature, and they are shown in figures 4(a) and (b), respectively. The low-temperature result (figure 4(a)) was measured with a SQUID, while the room-temperature one (figure 4(b)) was measured with an AGM. The M–H loops at both temperatures are typical of ferromagnetic materials. Complete saturation occurs within the applied field range, even though the field required for the saturation is much higher at 5 K than at room temperature. Indeed, the saturation field at 5 K is rather high, approximately 30 kOe, which is higher than the 1 kOe observed at room temperature. Considering this change in the saturation field, the magnetization data in the M–T curve shown in figure 3 are not the saturation values, particularly at low temperatures. Therefore, the initial decrease in *saturation* magnetization with increasing temperature will be greater than that shown in figure 3, resulting in a more concave M–T shape. Another notable feature observed from the M–H loops is the change in the hysteretic behaviour. The loop at 5 K is hysteretic with a coercivity of

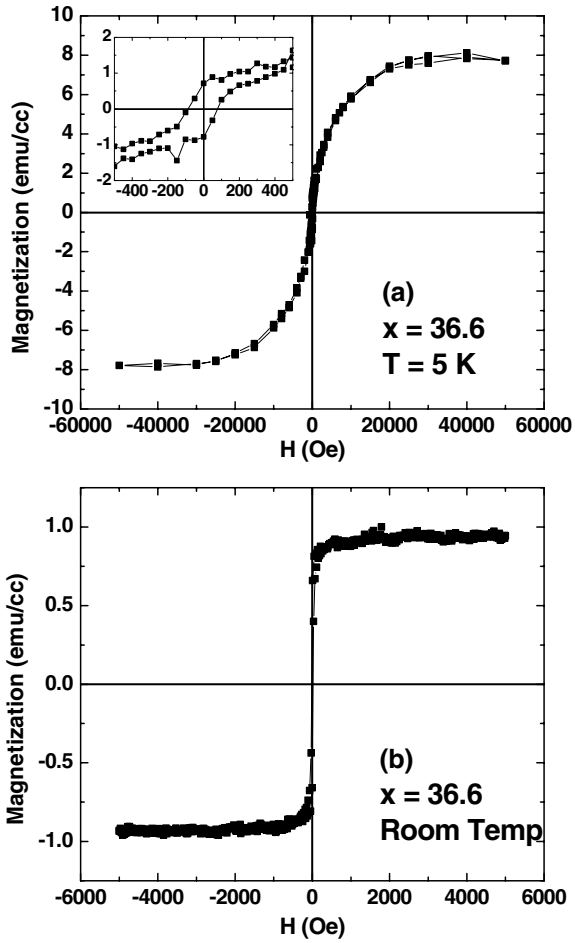

Figure 4. M–H hysteresis loops for the sample with $x = 36.6$. The loop in (a) was measured with a SQUID at 5 K and the result in (b) was measured with an AGM at room temperature. In the case of the loop at 5 K, the magnified part near the origin is shown in the inset.

approximately 85 Oe. However, this hysteretic behaviour disappears at room temperature, which is indicated by the zero coercivity and lack of remanence.

The large difference in magnetic behaviour as a function of the temperature is rather unusual, particularly the saturation field. In an effort to explain this behaviour, the temperature dependence of the in-plane components of the ac susceptibility was measured using a PPMS. Figure 5 shows the results of the in-phase component (real part) for the $x = 36.6$ sample. A constant dc bias field of 300 Oe was applied and the amplitude of the ac magnetic field was 5 Oe. The results were obtained over a wide frequency range of ac magnetic fields from 0.5 to 10 kHz. However, the results at low frequencies of 0.5 and 1 kHz are not shown here due to large scatter. A broad maximum is observed near 20 K in the temperature dependence of the ac susceptibility, which indicates a magnetic phase transition into a spin glass near that temperature ($T_f = 20$ K). Usually, the magnitude and position of the peak vary with the measured frequency, but no clear change is observed.

Let us now consider the magnetic properties of the sample with the highest x value, $x = 51.8$. M–T curves over a temperature range from 4 to 350 K are shown in figures 6(a) and (b),

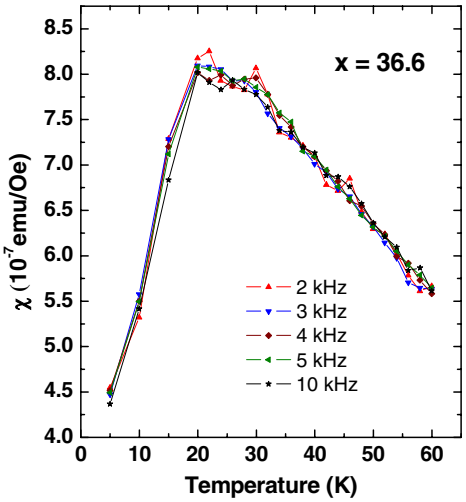

Figure 5. The temperature dependence of the ac susceptibility for the sample with $x = 36.6$ at various frequencies (2, 3, and 10 kHz). During the measurement, a constant dc bias field of 300 Oe was applied and the amplitude of the ac field was 5 Oe. Only the results for the in-phase component are shown.

respectively, at two different applied fields of 5 kOe and 30 Oe. Both results were measured with a SQUID at the zero-field-cooled condition. For the same sample, the M–H curves were measured at three different temperatures, 5, 150 and 300 K, and they are shown in figures 7(a)–(c), respectively. These three measured temperatures are indicated as vertical lines in the M–T curve shown in figure 6(b). At room temperature, an M–H curve was also measured with an AGM and the result is shown in figure 7(d). The most prominent feature from the results shown in figures 6 and 7 for the $x = 51.8$ sample is the significant increase in magnetization when compared with the samples with lower x values. The saturation magnetization at 5 K, as can be seen from figures 6(a) and 7(a), is approximately 250 emu cm^{-3}, which is much greater than the values (1–2.5 emu cm^{-3}) observed in similar Ge–Fe amorphous thin films with lower x values ($x \leqslant 35.9$) [7]. Even the saturation magnetization at $x = 51.8$ is much greater than the value of approximately 8 emu cm^{-3} obtained for the $x = 36.6$ sample at the same temperature of 5 K. The M–H curves in figures 7(a)–(d) show that saturation occurs at low applied fields, this being particularly true at low temperatures. Therefore, magnetization in the M–T curve at 5 kOe (figure 6(a)) represents the saturation magnetization. The saturation magnetization ($\sim$250 emu cm^{-3}) observed in the present thin film is very large indeed, and is comparable to that of 'ordinary' ferromagnetic materials. This large saturation magnetization strongly suggests the formation of Fe clusters. Similar to the sample with $x = 36.6$, a broad peak is observed at approximately 30 K in the M–T curve measured at a low applied field of 30 Oe ($T_f = 30$ K). It is possible that this type of broad peak in the temperature dependence of magnetization at a low applied field is related to a spin-glass phase. In order to check this, the temperature dependence of the ac susceptibility was measured under the same condition for the $x = 36.6$ sample (see figure 5) and the results are shown in figure 8. The inset shows a magnified part near T_f, where a very broad hump is clearly observed. As the frequency increases, the magnitude of the peak decreases while the position of the peak shifts towards a higher-temperature region. This type of frequency dependence near the broad peak is typical of a spin-glass phase.

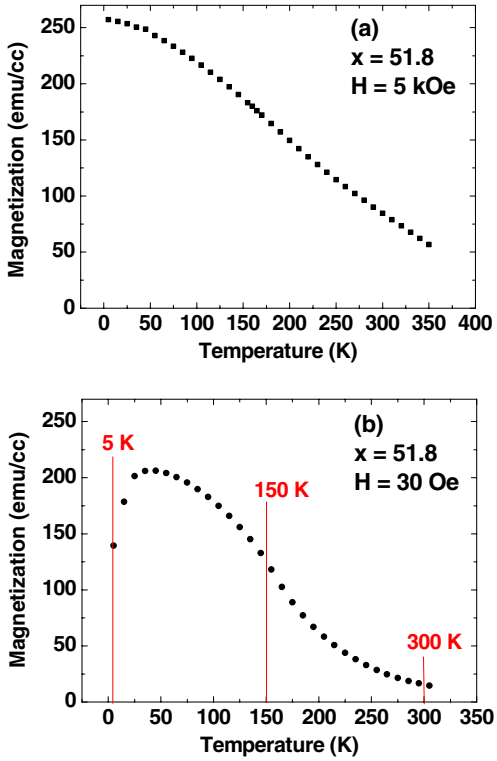

Figure 6. An M–T curve over a temperature range from 4 up to 350 K for the sample with $x = 51.8$. The result was obtained with a SQUID at the zero-field-cooled condition and at an applied field of (a) 5 kOe or (b) 30 Oe.

There is another peak in the temperature dependence of the ac susceptibility at 160 K, though much sharper than the one at 30 K. This peak might be related to the blocking of the superparamagnetic Fe precipitates for the following two reasons. First, the M–H loop at 150 K, which is just below the broad peak, is typical of ferromagnetic materials with good magnetic softness. The loop is characterized by the small coercivity (20 Oe), relatively high remanence ratio (>50%), and complete saturation at a small applied field (200–300 Oe). The second reason is related to the microstructure of the alloy. With a large amount of Fe, it is quite likely that the microstructure consists of Fe precipitates in an amorphous matrix, although this was not confirmed by HRTEM, as mentioned earlier in this section. The very large saturation magnetization also supports the presence of Fe precipitates. If this conjecture is true, then the M–H loops at temperatures above the peak (figures 7(c) and (d)) should show a superparamagnetic behaviour. However, it appears that these loops do not show this behaviour, mainly because of the hysteresis near the origin. The coercivity is estimated to be approximately 10 Oe in both cases. Considering the hysteretic M–H loop shape, it appears that these results do not support the superparamagnetic behaviour above the peak temperature. However, it is important to notice that the magnetization saturates very slowly and does not even saturate at the relatively high applied field of 2 kOe, although the coercivity is as low as 10 Oe. This type of magnetic behaviour is unusual if the magnetic phase is ferromagnetic. This is particularly true considering that the M–H loops at much lower temperatures (5 and 150 K) show complete saturation well below 600 Oe, which is the highest applied field during the

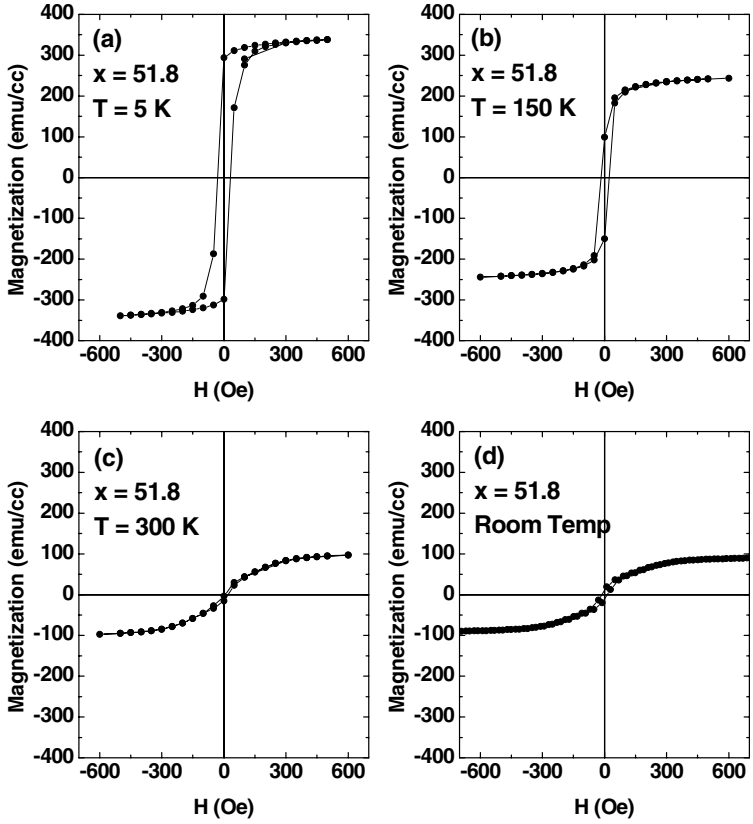

Figure 7. M–H curves measured with a SQUID for the sample with $x = 51.8$ at three different temperatures of (a) 5 K, (b) 150 K, and (c) 300 K. In (d), an M–H curve measured with an AGM at room temperature is also shown for the same sample. Note that the y-axis scales for the magnetization are identical to each other in order to better compare the change in magnetization as a function of temperature.

measurements. This is despite the fact that the coercivity is higher at these low temperatures: 30 Oe at 5 K and 20 Oe at 150 K.

Indeed, the M–H loops shown in figures 7(c) and (d), which are characterized by the slow increase in magnetization and high saturation field, are typical of superparamagnetism, with the exception of the non-zero coercivity. Therefore, one of the loops (at 300 K in figure 7(c)) was fitted using the Langevin function. The result is shown in figure 9. Two fitting parameters were used: the number of particles per unit volume and the magnetic moment per particle. As shown in figure 9, the agreement is reasonably good over the entire field range, with the exception of near the origin, which supports the superparamagnetic state above 160 K. If this is true, then the main issue to address is the non-zero coercivity. One possibility is the presence of large Fe clusters with blocking temperatures higher than room temperature. The small coercivity (10 Oe) also supports this. It is estimated from the Langevin fitting that the number of Fe precipitates per unit volume is 2.5×10^{17} cm^{-3} and the (average) magnetic moment per precipitate is 58 000 Bohr magnetons (μ_B). Since each Fe atom in the solid state possesses 2.2 μ_B, the average number of Fe atoms in each particle is calculated to be 26 000. A simple calculation shows that the number of Fe atoms residing in the precipitates is 6.5×10^{21} cm^{-3}. The total number of Fe atoms incorporated into Ge, which was measured

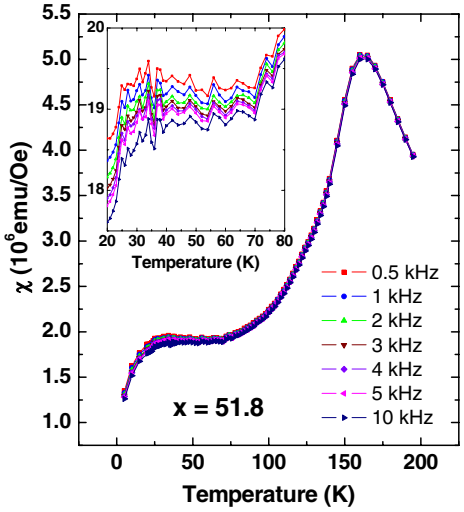

Figure 8. The temperature dependence of the ac susceptibility for the sample with $x = 51.8$ at various frequencies (0.5, 1, 2, 3, 4, 5, and 10 kHz). A constant dc bias field of 30 Oe was applied and the amplitude of the ac field was 5 Oe. The inset shows the magnified part near the spin freezing temperature where a large difference in the ac susceptibility is observed as a function of the measured frequency. Only the results for the in-phase component are shown.

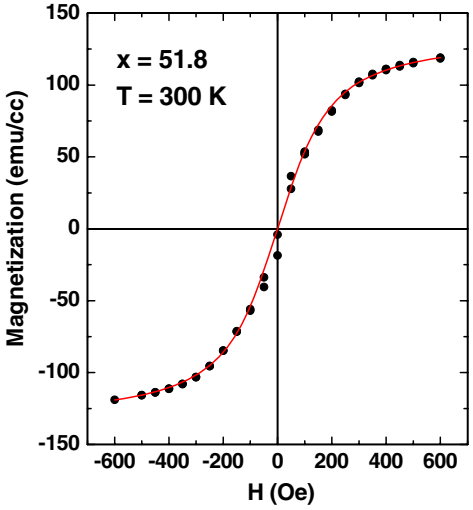

Figure 9. Fitting of the M–H curve for the sample with $x = 51.8$ at 300 K using the Langevin function. Two fitting parameters were used: the number of particles per unit volume and the magnetic moment per particle.

by Rutherford backscattering, is 2.7×10^{22} cm^{-3} at this composition ($x = 51.8$). Therefore, the fraction of Fe atoms in the precipitates is approximately 24% and the remainder (76%) is considered to be distributed uniformly in the amorphous matrix. This means that the *effective* composition of the amorphous phase corresponds to $x = 39.4$.

It is worth mentioning the spin-glass phase observed in these thin films in more detail. The existence of a spin-glass phase in II–VI DMSs doped with *Mn ions* is well documented in the

literature [11–17]. Well-known examples include (Cd, Mn)Te [11–13], (Pb, Mn)Te [14], (Hg, Mn)Te [15], (Zn, Mn)Te [16], and (Sn, Mn)Te [17]. These alloys are crystalline compounds. However, from a 'magnetic' point of view, the compounds represent an amorphous structure, because the Mn ions, which are the only magnetic elements, *randomly* fill the fcc sublattice sites formed within the compound structure. This refers to disordered magnetic doping in an otherwise regular host lattice. With the exception of (Sn, Mn)Te, the band gap is relatively large ($\sim$1 eV). Hence, the carrier (electrons or holes) concentration is small. This indicates that the indirect carrier-mediated exchange interactions (also called modified RKKY interactions) are very weak or even absent. Therefore, dominant exchange interactions between Mn ions are direct and short-ranged, usually between the nearest and next-nearest neighbours. In this type of II–VI DMS, a frustration, which is the origin of the spin-glass behaviour, occurs between the antiferromagnetically coupled Mn ions [18]. *Fe-doped* II–VI DMSs have received much less attention. In this case again, Fe ions randomly substitute for nonmagnetic cations. Therefore, from a 'magnetic' point of view, the Fe-doped compounds represent an amorphous structure, which is similar to the Mn-doped II–VI DMSs. However, the situation in Fe-doped DMSs is more complex due to the nonvanishing orbital momentum of Fe^{2+} ions ($S = 2$ and $L = 2$). Note that Mn^{2+} ions have spin-only magnetic moments ($S = 5/2$ and $L = 0$). It was reported that Fe ions only have a field-induced magnetic moment because the ground state is a magnetically inactive singlet, resulting in typical Van Vleck-type paramagnetism [19–21]. Despite this large difference, a similar spin-glass behaviour was observed in the Fe-doped DMSs, and the results were interpreted in a similar manner to Mn-doped DMSs [19–21].

Another class of DMSs showing a spin-glass behaviour is amorphous alloys containing magnetic ions [22–25], which are the subject of current investigation. In this case, magnetic ions are distributed randomly due to structural randomization. In the viewpoint of the random distribution of magnetic elements, this type of amorphous DMS is similar to II–VI DMSs. However, many important differences are known to result from the structural randomization, with one notable example being electrical conductivity [18]. The conduction electron elastic mean free path is reduced significantly by amorphization. This is the reason behind the significantly higher dopant concentration near the metal–insulator transition in amorphous alloys. The dopant concentration in amorphous alloys required to reach the metal–insulator transition ($\sim 10^{21}$ cm^{-3}) is many orders of magnitude larger than that in crystalline materials ($\sim 10^{17}$ cm^{-3}) [26]. A similar difference exists in the carrier concentration. In spintronics (spin-based electronics or spin electronics) applications, where DMSs are mainly used to inject spin into semiconductors without being hampered by the conductivity mismatch, the carrier concentration of interest needs to be near the metal–insulator transition [27–29]. Therefore, amorphous DMSs suitable for spintronic applications should have a high carrier density. However, again due to structural randomization, these carriers are localized [23]. This localization is further facilitated by large Coulombic carrier–carrier interactions due to the high carrier density and carrier–local moment interactions [23]. Although the carriers are localized, the localization length is rather long, and not confined to the atomic scale [23]. Therefore, unlike II–VI DMSs, there are indirect RKKY interactions in amorphous DMSs, mainly ferromagnetic coupling. With the presence of two opposite couplings in amorphous DMSs, direct antiferromagnetic and indirect ferromagnetic RKKY interactions, the frustration can be due to competition between these two couplings.

The complete saturation observed in the M–H loops in the spin-glass state (figure 4(a) at $x = 36.6$ and figure 7(a) at $x = 51.8$) is rather unusual. The M–H loop at 5 K (well below T_f) at $x = 36.6$ solely represents a spin-glass phase. However, this is not the case for the M–H loop at $x = 51.8$, where there are two different magnetic phases at the measured temperature (5 K): a spin-glass phase from an amorphous matrix with the effective Fe concentration of

$x = 39.4$ and a ferromagnetic phase from Fe precipitates. Of course, these Fe precipitates are responsible for the much higher level of (saturation) magnetization at $x = 51.8$. The low saturation fields observed in these thin films are totally different from the behaviour observed in amorphous Ge–Mn thin films, where the saturation is far from being reached even at 5 K and 50 kOe [6]. These low saturation values suggest that the direct antiferromagnetic exchange couplings between Fe ions in the amorphous Ge–Fe phase are much weaker than those between Mn ions in the amorphous Ge–Mn. Another important point to notice is the much smaller magnetization values in the present Ge–Fe system than in the Ge–Mn one. The value of (saturation) magnetization at $x = 36.6$ is approximately 8 emu cm^{-3} at 5 K and 50 kOe [7]. Under the same condition and a similar alloying content, the level of magnetization is much greater in the amorphous Ge–Mn thin films; for example, the magnetization is as high as 170 emu cm^{-3} at $x = 32.7$ (Mn content), even though saturation is far from being reached. The precise reason for this large difference is unclear. One possibility is the nonvanishing orbital momentum of Fe^{2+} ions resulting in a field-induced magnetic moment from a magnetically inactive singlet at the ground state [19–21], as was already discussed above.

4. Conclusions

Thin films of $Ge_{100-x}Fe_x$ (x in at.%) alloys with $x = 36.6$ and 51.8 were prepared by thermal co-evaporation onto oxidized Si substrates held at room temperature, and their magnetic phases were examined. At $x = 36.6$, the microstructure consists of a single amorphous phase. The magnetic phase at room temperature appears ferromagnetic [7] but a phase transformation into a spin-glass phase occurs at 20 K. At $x = 51.8$, a more complicated behaviour is observed, mainly due to the presence of Fe precipitates in an amorphous matrix. The effective composition of the amorphous phase from an analysis based on the superparamagnetism is estimated to be $x = 39.4$, and this amorphous phase shows a magnetic behaviour similar to the $x = 36.6$ sample except for the slightly higher spin freezing temperature of 30 K. This magnetic behaviour is superimposed with a superparamagnetic behaviour, due to Fe precipitates, with a blocking temperature of 160 K. Compared with the Ge–Mn system, the saturation field is significantly small, indicating that direct antiferromagnetic exchange couplings between Fe ions in the amorphous Ge–Fe are much smaller than those among Mn ions in the amorphous Ge–Mn. Much smaller magnetization values are observed in the Ge–Fe system than in the Ge–Mn one. This is possibly due to the nonvanishing orbital momentum of Fe^{2+} ions resulting in a field-induced magnetic moment from a magnetically inactive singlet at the ground state [19–21].

Acknowledgments

This work was supported by the Korean Ministry of Science and Technology through the National Research Laboratory program and also by the Research Center of Advanced Magnetic Materials at CNU. The authors wish to thank W B Paek for her help in structural characterization.

References

[1] Dietl T, Ohno H, Matsukura F, Cibert J and Ferrand D 2000 *Science* **287** 1019
[2] Park Y D, Hanbicki A T, Erwin S C, Hellberg C S, Sullivan J M, Mattson J E, Ambrose T, Wilson A, Spanos G and Jonker B T 2002 *Science* **295** 651

[3] Choi S, Hong S C, Cho S, Kim Y, Ketterson J B, Jung C-U, Rhie K, Kim B-J and Kim Y C 2002 *Appl. Phys. Lett.* **81** 3606
[4] Kioseoglou G, Hanbicki A T and Jonker B T 2003 *Appl. Phys. Lett.* **83** 2716
[5] Paek W B, Kim J and Lim S H 2004 *Phys. Status Solidi* b **241** 1521
[6] Song S H, Lim S H, Jung M H, Santos T S and Moodera J S 2006 *J. Korean Phys. Soc.* at press
[7] Song S H and Lim S H 2006 *J. Magn. Magn. Mater.* **304** 64
[8] Song S H, Jung M H and Lim S H 2006 unpublished results
[9] Massalski T B (ed) 1990 *Binary Alloy Phase Diagrams* 2nd edn, vol 2 (Metals Park, OH: American Society for Metals) p 1706
[10] Das Sarma S, Hwang E H and Kaminski A 2003 *Phys. Rev.* B **67** 155201
[11] Mauger A, Villian J, Zhou Y, Rigaux C, Bontemps N and Ferre J 1990 *Phys. Rev.* B **41** 4587
[12] Geschwind S, Huse D A and Devlin G E 1990 *Phys. Rev.* B **41** 4854
[13] Bertrand D, Mauger A, Ferre J and Beauvillain P 1992 *Phys. Rev.* B **45** 507
[14] Tholence J L, Benoit A, Mauger A, Escorne M and Triboulet R 1984 *Solid State Commun.* **49** 417
[15] Zhou Y, Rigaux C, Mycielski A, Menant M and Bontemps N 1989 *Phys. Rev.* B **40** 8111
[16] Shand P M, Christianson A D, Pekarek T M, Martinson L S, Schweitzer J W, Miotkowski I and Crooker B C 1998 *Phys. Rev.* B **58** 12876
[17] Escorne M, Godinho M, Tholence J L and Mauger A 1985 *J. Appl. Phys.* **57** 3424
[18] Binder K and Young A P 1986 *Rev. Mod. Phys.* **58** 801
[19] Swagten H J M, Twardowski A, de Jonge W J M and Demianiuk M 1989 *Phys. Rev.* B **39** 2568
[20] Twardowski A 1990 *J. Appl. Phys.* **67** 5108
[21] Chen Y F, Chou W C and Twardowski A 1995 *Solid State Commun.* **96** 865
[22] Hellman F, Tran M Q, Gebala A E, Wilcox E M and Dynes R C 1996 *Phys. Rev. Lett.* **77** 4562
[23] Zink B L, Janod E, Allen K and Hellman F 1999 *Phys. Rev. Lett.* **83** 2266
[24] Hellman F, Queen D R, Potok R M and Zink B L 2000 *Phys. Rev. Lett.* **84** 5411
[25] Zink B L, Preisler V, Queen D R and Hellman F 2002 *Phys. Rev.* B **66** 195208
[26] Furdyna J K 1982 *J. Appl. Phys.* **53** 7637
[27] Smith D L and Silver R N 2001 *Phys. Rev.* B **64** 045323
[28] Albrecht J D and Smith D L 2002 *Phys. Rev.* B **66** 113303
[29] Albrecht J D and Smith D L 2003 *Phys. Rev.* B **68** 035340